# Nucleation Experiments with Monodisperse NaCl Aerosols

D. J. ALOFS,[1] M. B. TRUEBLOOD, D. R. WHITE[2] AND V. L. BEHR[1]

*Cloud Physics Research Center, University of Missouri-Rolla, Rolla 65401*

(Manuscript received 18 January 1979, in final form 19 May 1979)

ABSTRACT

Nucleation experiments with monodisperse NaCl aerosols showed good agreement with the Köhler theory relating the critical super-saturation $S_c$ to the dry size. Aerosols produced by condensing NaCl showed the same $S_c$ as those produced by evaporating aqueous NaCl solution droplets. This indicates that if there is an energy barrier in going from a dry NaCl particle to a solution droplet, this energy barrier is small. The fact that the evaporation aerosol particles are cubical crystals and the condensation aerosols are amorphous spheres is shown to make no difference in the nucleation threshold.

The investigation also gives insights into the performance of the equipment used, especially the commercial electrostatic aerosol classifier and the vertical flow thermal diffusion chamber developed in this laboratory. When operating this chamber in the isothermal mode, a 36% upper limit was found on the uncertainty in $S_c$ due to index of refraction sensitivity in sizing the water drops. Within this range of uncertainty, the isothermal mode data agreed with the Köhler theory.

## 1. Introduction

The Graduate Center for Cloud Physics Research at the University of Missouri-Rolla is entering the final phase of development of a cooled-wall expansion cloud chamber designed for simulation studies of cloud microphysics. The value of supersaturation $S$ in this chamber is calculated from the initial relative humidity, and a knowledge of the thermodynamic changes that occur during the expansion, including changes resulting from the heat release and vapor depletion due to droplet growth. At the time of this writing, the performance of the simulation chamber is being experimentally investigated by using test aerosols of monodisperse NaCl particles. Since these particles all have about the same size and chemical composition, they should all have the same critical supersaturation $S_c$ and in the simulation chamber they should produce a monodisperse cloud of droplets which undergo a marked increase in growth rate when the $S$ in the chamber exceeds $S_c$.

This paper describes the aerosol-generation facility developed for use with the simulation chamber, and describes experiments performed to verify the monodispersity and to determine the $S_c$ of the aerosols, using the vertical flow thermal diffusion chamber developed by Alofs and co-workers (Alofs, 1978). The experimental data also provides valuable information on the resolution of this thermal diffusion chamber.

Two different aerosol generating techniques were used for these investigations. In the first, NaCl is vaporized, mixed with air in a steady flow process, and subsequently cooled so that the NaCl vapor condenses. In the second technique, a solution of NaCl in water is atomized and the water in the droplets subsequently evaporates to leave NaCl particles. The output from either of these generators is then made monodisperse by passing it through a Thermo Systems Inc. Model 3071 electrostatic classifier,[3] developed by Liu, Whitby, and co-workers (Liu and Pui, 1974a, Knutson and Whitby, 1975).

The equipment for the evaporation technique is much simpler than for the condensation technique, but it was believed possible that the two techniques might give different nucleation thresholds. One difference between the two techniques is that evaporation produces particles which are cubical crystals, whereas condensation produces amorphous spheres (Matijevic *et al.*, 1963). Another possible difference between the techniques concerns the possibility of surface impurities on the aerosol particles. One might expect that there would be more contamination with the evaporation technique because all of the impurities in the water end up on the salt particles finally produced, whereas in the condensation technique, there are no impurities due to such water. Since impurities having surface active characteristics are known to influence droplet growth rates (Derjaguin *et al.*, 1971; Podzimek and Saad, 1975), it was believed important to be able to compare aerosol particles generated by two completely different means. Measurements of droplet growth rate

[1] Also Department of Mechanical Engineering.
[2] Also Department of Engineering Mechanics.
[3] Thermo Systems Incorporated, 500 Cardigan Road, St. Paul, MN 55165.

0021-8952/79/091106-12$07.00

are underway for both aerosols and will be presented in a separate report.

The experiments described in this report are quite similar to those described by Gerber *et al.* (1977). They used an evaporation aerosol generation technique, and then used an electrostatic classifier together with a Goetz centrifuge to produce monodisperse particles. They then determined $S_c$ using the Naval Research Lab static horizontal thermal diffusion chamber. The experimental values of $S_c$ versus dry particle size agreed well with results from the Köhler equations (Pruppacher and Klett, 1978). Considering the fact that the Köhle equations are used extensively in cloud microphysics calculations and that previous attempts to verify the Köhler theory had failed, their experiment was a big breakthrough. One of the contributions of this paper is that we repeat their experiment at a different laboratory, using similar but not identical equipment, and get the same good agreement with theory.

Another contribution of this paper concerns the question of whether or not there is an energy barrier in going from a dry NaCl particle to a solution droplet. Knight (1971) presented a photograph of tiny liquid water drops resting on the surface of NaCl crystals and not being absorbed. He suggested an energy barrier exists that is not taken into account by the Köhler equations. The transition between solution droplet and salt crystal is known to exhibit a hysteresis effect (Winkler and Junge, 1972) such that for NaCl, a dry particle does not take up water until the humidity reaches 75%, whereas a wet particle does not give up all of its measurable water until the humidity is lowered below 50%. However, perhaps in these hysteresis experiments the supposedly dry particles really contain a small amount of water too small to be measured in the experiment. Perhaps then a truly dry particle would need a humidity higher than 75% before it takes up water. Thus we believe that neither the experiments of Gerber *et al.* (1977) nor those by Winkler and Junge (1972) rule out the possibility of an energy barrier for a completely dry particle. Since the NaCl particles prepared by the condensation techniques are initially dry, it was believed possible that an energy barrier might show up in our experiments; thus the NaCl particles produced by condensation might give a higher $S_c$ than those produced by evaporation.

## 2. Description of the condensation aerosol generator

Fig. 1 is a schematic of the condensation aerosol generator, which utilizes a series of furnaces, in accord with the investigation of Espenscheid *et al.* (1964). About 5 g of reagent grade NaCl is placed in a ceramic boat 9 cm long×8 mm wide×0.6 mm deep. This boat, which is open at the top, is placed inside a ceramic mullite tube, 2.5 cm inside diameter × 223 cm long. The ceramic tube passes through four electric furnaces,

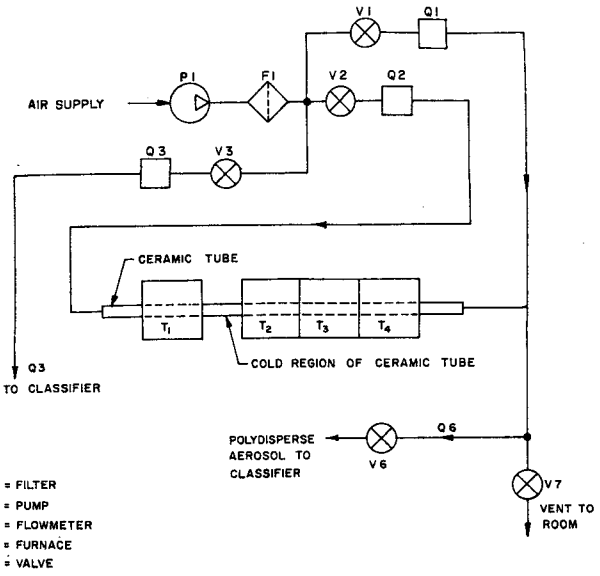


FIG. 1. Schematic of the condensation aerosol generator.

which maintain the respective lengths of the ceramic tube at the desired temperatures. Each of the furnaces has a thermocouple located on the outside surface of the ceramic tube, midway along the length of each furnace. Manual control of the furnace power settings was found to be unsatisfactory, so automatic control circuits were built for each furnace. With these control circuits, the temperatures are stable to within ±1°C.

The first furnace, denoted by $T_1$ in Fig. 1, contains the boat of NaCl midway along the 65 cm length of the furnace. Typically, $T_1$ was held at 730°C. Filtered air flows through the ceramic tube, and mixes with the NaCl vapor. This flow, denoted by $Q_2$ in Fig. 1, is typically 1.5 $\ell$ min$^{-1}$.

The mixture of air and NaCl vapor then passes through a cooler region of the ceramic tube, which is a region 8 cm long where the tube is exposed to room air. The inside surface temperature of the tube in this cooler region was measured and found to be 300°C at the coolest spot. Within the cool region, the NaCl vapor undergoes nucleation. Kitani and Ouchi (1967) believed that this first nucleation is homogeneous nucleation. Another possibility is heterogeneous nucleation occurring on ions, or on particles passing through the filter (F1, Fig. 1). A particle count with a Gardner Counter[4] however, shows zero count downstream of the filter. Moreover, the concentration of ions in the atmosphere is only about $5\times10^3$ cm$^{-3}$ even near cities (Fleagle and Businger, 1963, p. 117), whereas the aerosol concentrations are generally above $10^6$ cm$^{-3}$. Whether this nucleation is homogeneous or heterogeneous, the important fact here is that the aerosol produced from the first nucleation process is very polydisperse (Matijević *et al.*, 1962, 1963).

[4] Gardner Associates, 3435 Carman Road, Schenectady, NY 12302.

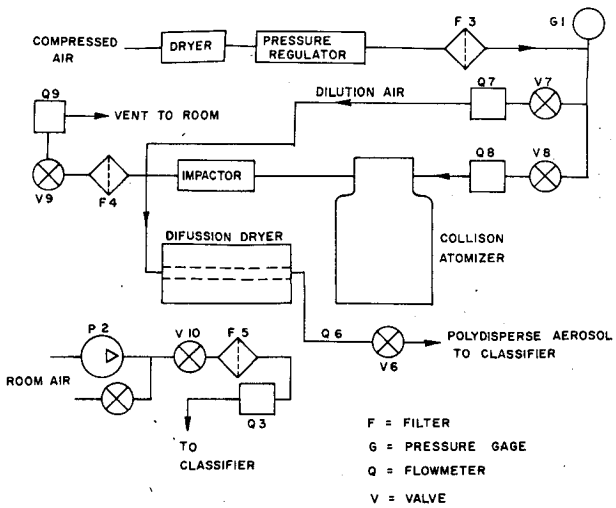


FIG. 2. Schematic of the evaporation aerosol generator.

Kitani and Ouchi (1967) found that by revaporizing and then recondensing this aerosol, a more monodisperse aerosol can be obtained. Making use of their discovery, we therefore pass the aerosol into a second furnace, denoted $T_2$ (Fig. 1), where the temperature is typically 870°C. Since the second furnace is hotter than the first furnace, it might at first appear that the aerosol would be completely vaporized in passing through the second furnace. It should be considered, however, that in the first furnace the NaCl is continuously heated, whereas in the second furnace the time for evaporation is limited by the residence time in the furnace. This time limitation probably explains why a residue aerosol emerges from the second furnace to act as nuclei for condensation in the downstream regions of the generator.

The aerosol then flows into furnaces $T_3$ and $T_4$, whose purpose is to give a slower cooling rate than would otherwise exist. Furnace $T_3$ is between 25 and 50°C cooler than $T_2$, depending on what average particle size is desired. This same temperature drop is repeated from furnace $T_3$ to furnace $T_4$. It was found that the rate of cooling in these regions greatly influences the average size of the particles produced, as discussed in Section 5.

After leaving the last furnace, the aerosol passes through the last 10 cm length of the ceramic tube, which is exposed to room air. The aerosol is then diluted with filtered air, denoted by $Q_1$ in Fig. 1. This dilution flow is one of the parameters which is varied to control aerosol concentration, but typically, lies between 1.0 and 10.0 $\ell$ min$^{-1}$.

## 3. Description of the evaporation aerosol generator

The set up for the evaporation generator is shown in Fig. 2, and is similar to that used by Liu *et al.* (1975). Compressed air passes through a silica gel dryer, and then through a pressure regulator set for 25 psi gage. Part of the flow ($Q_8$, 2.5 to 4 $\ell$ min$^{-1}$) then goes into a standard Collision atomizer (May 1973), the remainder ($Q_7$, 9 $\ell$ min$^{-1}$) serves as dilution flow. The aerosol then passes through an impactor to remove the largest drops. Part of this flow is discarded, the remainder passing through a diffusion dryer. The diffusion dryer consists of two concentric tubes 64 cm long. The inner tube (2 cm diameter) is made of fine-mesh screen and the outer tube (8 cm inside diameter) is made of Plexiglass. The annular volume between the tubes is filled with dry silica gel. Thus the air passing through the inside tube looses water vapor by diffusion to the silica gel, but the air itself does not pass through the silica gel. After passing through the diffusion drier, the air then enters the bipolar charger and finally, the classifier.

The concentration of the salt solution put into the atomizer was determined by a graph presented by Liu and Pui (1974a). The criterion used is that the particles entering the classifier have a geometric mean size equal to the size of the desired monodisperse aerosol, as long as the desired monodisperse aerosol was not $> 0.05$ $\mu$m diameter. For producing monodisperse aerosol above 0.05 $\mu$m, the classifier was set for the desired size, but the salt solution which gave 0.05 $\mu$m average size was used. This resulted in lower aerosol concentrations coming out of the classifier, but was necessary because the atomizer tended to plug up when using more concentrated salt concentrations, corresponding to larger salt particles. Both Liu and Pui (1974a) and ourselves found that the size distribution from the generator is approximately log-normal. Reagent grade NaCl and doubly distilled water were used to make up the salt solutions.

## 4. Description of the electrostatic classifier

Fig. 3 provides a schematic of the classifier. The aerosol from either generator passes through the bipolar

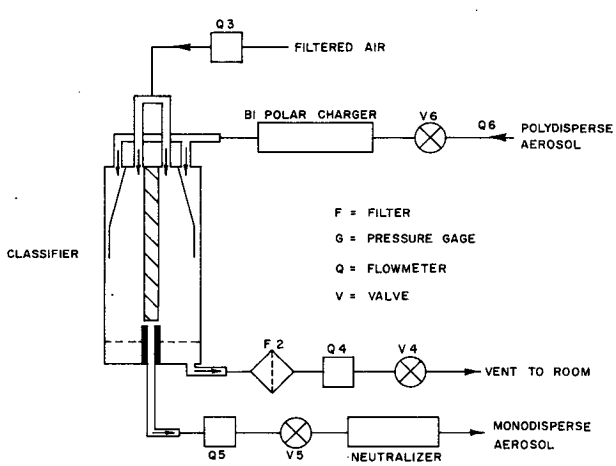


FIG. 3. Schematic of the electrostatic classifier.

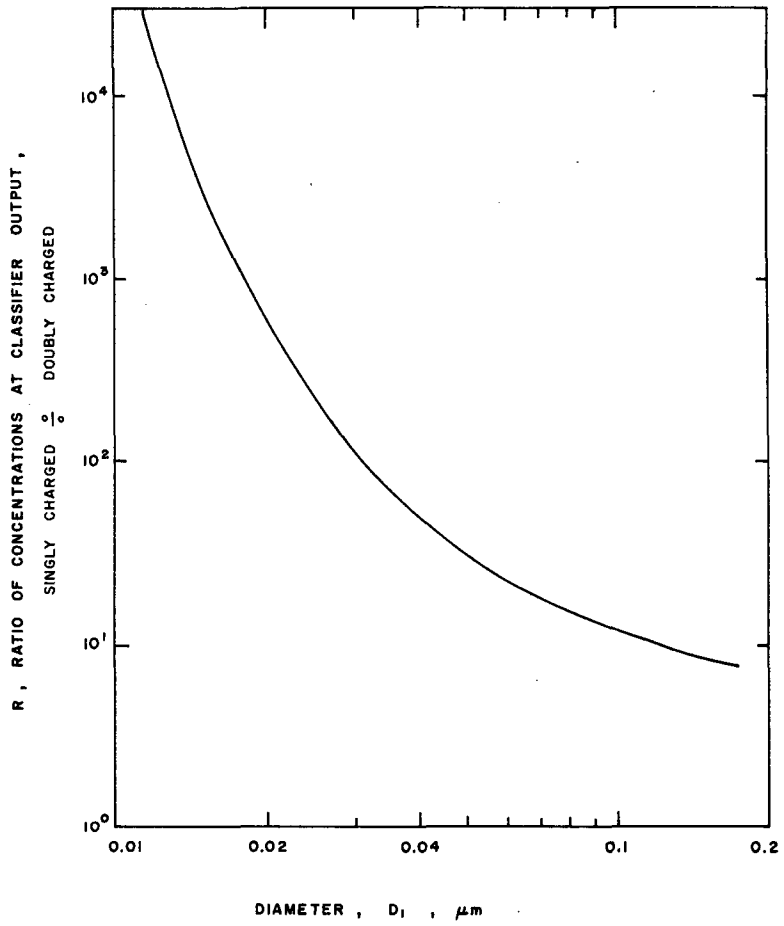


FIG. 4. The calculated ratio $R$ of singly charged particle concentration divided by doubly charged particle concentration, both at the output of the classifier. The diameter $D_1$ is the size of the singly charged particles. The assumption $N_1=4N_2$ is included, as described in the text.

charger, which is a Krypton 85 radioactive source that imparts a charge distribution to the aerosol particles. The charge distribution has been found to follow Boltzmann's law for particles $> 0.01$ $\mu$m diameter (Liu and Pui, 1974b). Thus the fractions of the particles having a given charge is a known function of size.

The main component of the electrostatic classifier consists of an outer cylinder at zero electrical potential, and a concentric inner rod kept at a negative potential in the range 20–10 000 V. Two streams of air are introduced into the annulus region at the top of the classifier (Fig. 3). The smaller flow, typically 9% of the total, is the aerosol flow $Q_6$, which comes from the charger and is introduced near the outer cylinder. The other flow is filtered air $Q_3$. The inlet systems are designed such that ideally these two air streams do not mix, but instead flow side by side down through the classifier. Near the bottom of the chamber, a small flow $Q_5$ is withdrawn through a slit in the rod. $Q_5$ is typically 9% of the total flow. The rest of the air $Q_4$ is withdrawn through a separate port and discarded.

The aerosol particles which have a positive charge are deflected inward toward the rod. Those possessing the same mobility arrive at the central rod at very nearly the same axial location. Those with a specific mobility arrive at the slit and become incorporated in the exit flow $Q_5$. Thus the exit flow consists of a fairly monodisperse aerosol. Limitations on the degree of monodispersity are now discussed.

One limitation on monodispersity is the charge distribution on the particles. If the classifier is set to pass particles of size $D_1$, having one positive unit charge, it will also pass particles of larger size $D_2$, carrying two positive charges. This is because the $D_2$ and $D_1$ particles have the same electrical mobility, $Z_p$ and experience an identical deflection path in the electric field of the classifier. By using a table of mobility values (Fuchs, 1964) one can calculate $D_2$ as a function of $D_1$.

In the experiments of Gerber *et al.* (1977) the problem of the doubly charged particles was solved by using a centrifuge set to remove all particles larger than $D_1$.

In our investigations, this problem is solved by controlling the aerosol size distribution going into the classifier, such that the concentration $N_1$ of particles in the range $D_1 \pm \Delta D_1$ is at least four times larger than the concentration $N_2$ of particles in the range $D_2 \pm \Delta D_2$. Here $\Delta D$ is merely notation for the resolution of the classifier. Now let $f_1$ be the fraction of $N_1$ that carry a single positive unit charge, and let $f_2$ be the fraction of $N_2$ that carry a double positive charge. The Boltzmann equation (Liu and Pui, 1974b) is used to calculate $f_1$ and $f_2$. Now for the classifier output aerosol, let the respective concentrations of singly and doubly charged particles be denoted by $n_1$ and $n_2$. Then $n_1 = N_1 f_1$ and $n_2 = N_2 f_2$. The ratio $R = n_1/n_2$ is plotted in Fig. 4 as a function of $D_1$ assuming $N_1 = 4N_2$. It can be seen that doubly charged particles are not much of a problem when $D_1 < 0.1$ $\mu$m.

Another limitation on monodispersity is the finite thickness of the air stream which carries the aerosol particles into the classifier. Consider the case where the polydisperse aerosol inflow $Q_6$ equals the monodisperse aerosol outflow $Q_5$. The analysis of Knutson and Whitby (1975) shows that for this case (which was used throughout the present investigation) the classifier will have a triangular transfer function. The transfer function $\Omega$ is the ratio of the output concentration of particles with mobility $Z$, to the input concentration of particles with the same $Z$. Thus a plot of $\Omega$ versus $Z$ is a triangle, with $\Omega = 0$ for $Z < Z_p - \Delta Z$, a linear rise in $\Omega$ from $Z_p - \Delta Z$ to $Z_p$, a linear decline in $\Omega$ from $Z_p$ to $Z_p + \Delta Z$, and $\Omega = 0$ for $Z_p > Z_p + \Delta Z$. Knutson and Whitby derive the following formula

$$\frac{\Delta Z}{Z_p} = \frac{Q_6}{Q_3}, \tag{1}$$

where $Q_6$ is the aerosol flow and $Q_3$ is the filtered air flow. In the present investigations $Q_6/Q_3 = 0.1$, so that the classifier would have a band width of $\pm 10\%$ in $Z$ due to this effect alone.

A third limitation on monodispersity is due to the fact that it is impossible to prevent a finite amount of mixing between the two air streams in the classifier. Moreover, in deriving Eq. (1) it is assumed that the thickness of the aerosol stream is the same all around the circumference of the classifier. We have experimental evidence indicating that this angular uniformity is poor, because when taking apart the classifier for cleaning, we always notice that the salt deposits on the outer cylinder are substantially nonuniform: the deposits show an angular pattern of eight stripes running the length of the tube. Thus, it should be expected that $\Delta Z$ will be larger than the idealized representation given by Eq. (1).

## 5. Effect of temperatures and flow on the particle size distribution from the condensation generator

A series of experiments were performed to determine how the various operating parameters of the condensation aerosol generator influence the aerosol size distribu-

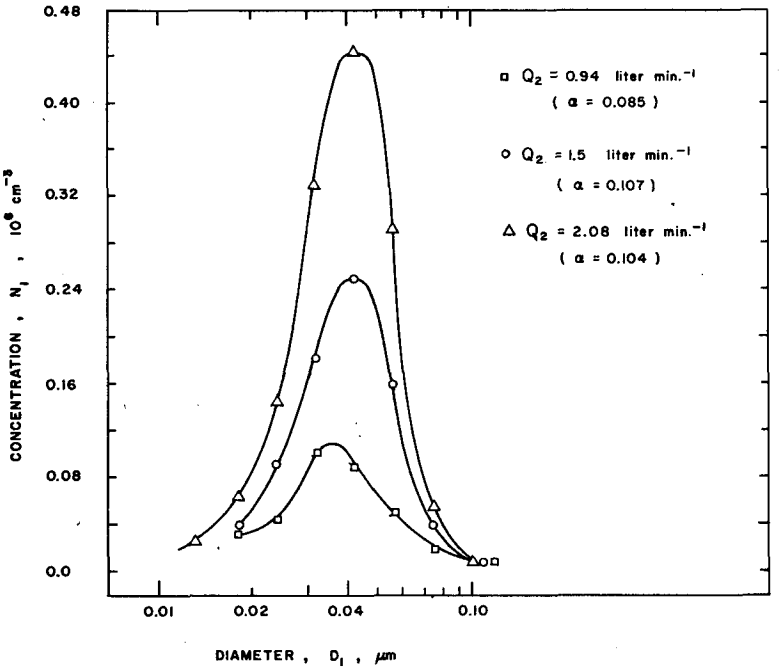


FIG. 5. The effect of varying $Q_2$ on the particle size distribution from the condensation aerosol generator $Q_1 = 2.0$, $Q_3 = 20$, $Q_6 = 2$ $\ell$ min$^{-1}$, $T_1 = 735$, $T_2 = 871$, $T_3 = 825$, $T_4 = 783$°C.

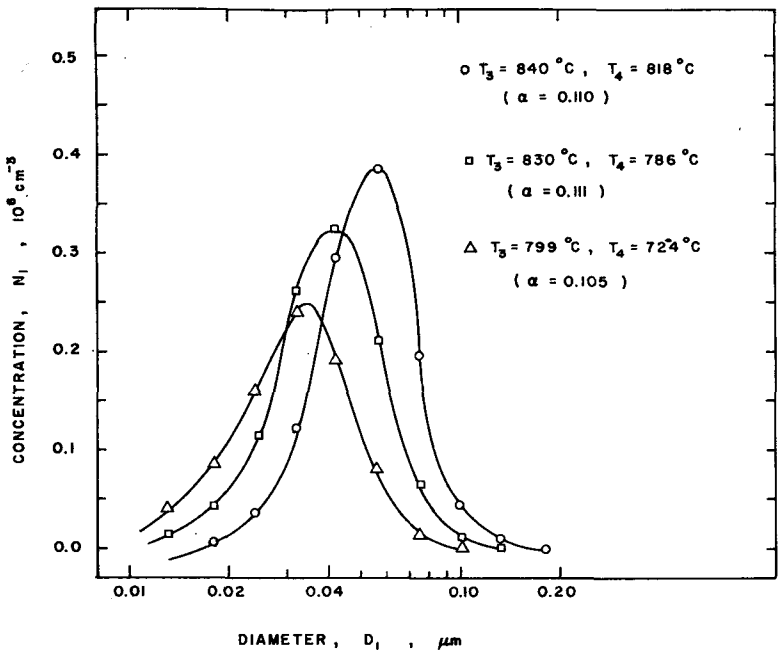


FIG. 6. The effect of varying $T_3$ and $T_4$ on the particle size distribution from the condensation aerosol generator $Q_1=1.0$, $Q_2=1.5$, $Q_3=20$, $Q_6=2$ $\ell$ min$^{-1}$, $T_1=732$, $T_2=871$°C.

tion. To measure the size distribution, the classifier was used. The output of the classifier was measured with a Gardner counter as a function of the classifier rod voltage. This procedure is referred to as a classifier voltage sweep. Hoppel (1978) has described a rigorous procedure for analyzing such data in order to extract the input size distribution. However, in this investigation Hoppel's procedure is not used because the size distributions are sufficiently narrow that a simpler analysis suffices. Recalling the notation of Section 4, the Gardner counter measures the concentration $n_1+n_2=N_1f_1+n_2f_2$. When analyzing the data from a voltage sweep, the procedure is to neglect particles with more than one charge ($n_2$). This simplification is justified by the large value of $R$ as discussed in Section 4. Then $N_1$ can be obtained by dividing $n_1$ by $f_1$. Recall that $n_1$ is the concentration of particles passed by the triangular transfer function $\Omega$ of the classifier. Roughly, $N_1$ is the concentration of particles in the size range $D_1\pm\Delta D_1$, where the value of $\Delta D_1$ is between 10 and 20% of $D_1$.

The size distributions thus measured were found to be approximately log normal. The relative geometric standard deviation $\alpha$ of the distributions usually had a value near 0.1. Since aerosols with $\alpha\leqslant 0.2$ have been termed monodisperse (Fuchs and Sutugin, 1966), these results show that the aerosol going into the classifier is already fairly monodisperse. It is also interesting to note that other investigations with condensation generators yield $\alpha$ near 0.1 (Kitani and Ouchi, 1967; Kerker, 1975; Espenscheid *et al.*, 1964). None of these other generators, however, produced particles as small as those produced in the present investigation.

Fig. 5 shows the result of varying $Q_2$, the flow through the ceramic tube, while keeping the other parameters constant at the values indicated on the legend. It can be seen from Fig. 5 that varying $Q_2$ does not affect $\alpha$, nor does it affect the geometric mean diameter ($D_g$). However, $Q_2$ is seen to affect concentrations, higher flows giving higher concentrations. The higher concentrations would indicate more particles being formed during the first condensation process. This could be due either to a higher cooling rate or to a larger supply of vapor because of better ventilation across the boat of salt.

Fig. 6 shows the effect of varying the temperature drop in the last furnaces, i.e., varying $T_2-T_3$ and $T_3-T_4$. As these values decrease, the cooling rate of the vapor decreases and it is seen that larger particles are formed. Again, $\alpha$ is not noticeably influenced.

Fig. 7 shows the effects of varying, $T_1$ the temperature of the first furnace. It can be seen that $\alpha$ is not greatly effected, but the particle concentration and values of $D_g$ are effected.

We do not have one unified explanation for all the behavior exhibited in Figs. 5, 6 and 7. We are surprised that $\alpha$ remained contstant throughout and that $D_g$ was not a function of $Q_2$ (Fig. 5). Therefore, these data were utilized merely as an empirical guide for setting up the generator to get the concentrations and sizes desired. For example, the size was controlled chiefly

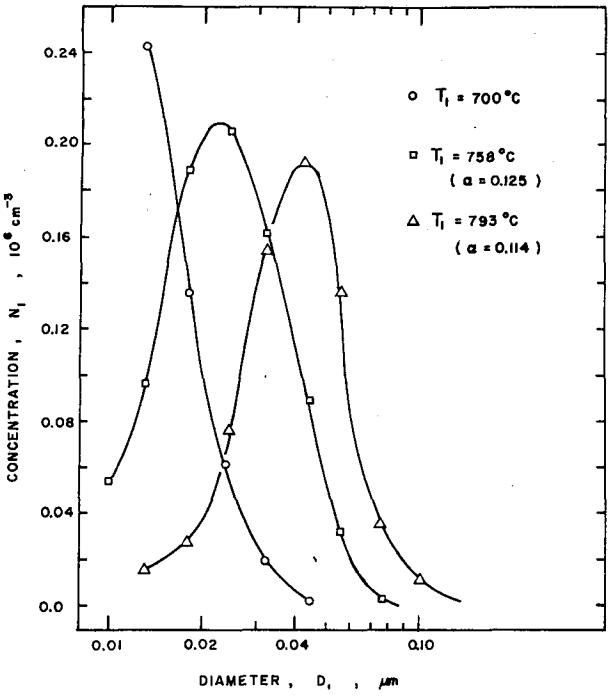


FIG. 7. The effect of varying $T_1$ on the particle size distribution from the condensation aerosol generator $Q_1=2$, $Q_2=1.5$, $Q_3=20$, $Q_6=2$ ℓ min$^{-1}$, $T_2=870$, $T_3=822$, $T_4=781$°C.

by varying the cooling rate in the last ovens, in accord with the behavior seen in Fig. 6.

One other effect that should be mentioned is depletion of the salt in the boat. The furnaces and the air flow were left running 24 h day$^{-1}$, and it was found that about once very seven days the salt had to be replaced. As the salt depleted the aerosol concentration and $D_0$ decreased slowly. These decreases were offset by increasing $T_1$ by ~40°C once during the middle of the 7-day period.

## 6. The temperature sweep procedure

The nucleation experiments consisted of determining the critical supersaturation $S_c$ of the monodisperse NaCl aerosols. To do this the vertical continuous flow thermal diffusion chamber (CFD) developed by Alofs and co-workers was employed. This instrument and its performance characteristics have recently been described in detail (Alofs, 1978) and therefore only a brief description of it is given here.

The CFD consists of two vertical plates, 100 cm long in the vertical direction and 13 cm wide, with a 0.8 cm spacing between the plates. A temperature difference is generally maintained between the plates, and distilled water is supplied to filter paper on their surfaces. The temperature dependence of the equilibrium vapor pressure of water is such that a supersaturation is produced in the air–water vapor mixture contained between the plates. The supersaturation profile is nearly parabolic, with the supersaturation equal to zero at each plate, and a maximum supersaturation $S$ midway between the plates.

Filtered air and the test aerosol are injected at the top of the TDC in such a way that the aerosol remains in a narrow stream centered between the plates as the aerosol passes through the chamber. Both the active nuclei $S_c < S$ and the haze nuclei $S_c > S$ experience growth in the CFD, however, the active nuclei produce larger water drops than the haze nuclei.

At the bottom of the chamber the water drops are drawn into a optical particle counter (OPC), where the light scattered from individual water drops is measured in order to determine the droplet size distribution. The diameter (μm) of the largest haze drop is estimated by theory to equal 0.138 $S_c^{-1}$, where $S_c$ is in percent (Alofs, 1978). Therefore, all drops larger than this are counted as coming from active nuclei. In the present investigations two CFD were employed, each with a different commercial brand of OPC. The first used a Royco[6] model 225 OPC, the second used a Climet[6] model 201 OPC.

In order to determine $S_c$ for the monodisperse aerosols, the temperature of the colder plate was slowly changed with time, while all the other parameters were held fixed. This procedure is referred to as a temperature sweep, and required about 30 min to complete. Temperature sweeps were made in both directions, that is, with $S$ both increasing and decreasing with time, and no difference in the resulting $S_c$ was observed. This indicates that the rate of temperature change was sufficiently slow to insure that various thermal lags in the cold plate were negligible.

For the sake of completeness, the values of the quantities held fixed during the temperature sweeps are now specified. The hot plate temperature was always 25°C. The aerosol flow rate into the CFD was 8.5 cm$^3$ min$^{-1}$, and the flow into the OPC was 0.5 ℓ min$^{-1}$. The value of the filtered air-flow rate, which determines the residence time in the CFD, depended on the aerosol being tested. For aerosols with a $D_1$ of 0.022, 0.050 and 0.10 μm, the values were 8, 5 and 3 ℓ min$^{-1}$, respectively. The aerosol from the classifier was always diluted in a steady flow process to a concentration below 100 cm$^{-3}$ before passing it into the CFD.

## 7. The isothermal procedure

The temperature sweep procedure described above was used for aerosols with $S_c \geq 0.1\%$. However, experiments were also conducted in the range $S_c < 0.1\%$, and for these experiments the CFD was operated in the isothermal mode. In this mode the two plates are kept at the same temperature, 25°C, so that a relative humidity of 100% is formed between the plates. The

[6] Royco Instruments, 141 Jefferson Drive, Menlo Park, CA 94025.

[6] Climet Instruments Company, 1320 W. Colton Avenue, Redlands, CA 92373.

total flow in the CFD is reduced such that the residence time of the aerosol sample increases to 200 seconds. This time is sufficient so that nuclei with $S_c > 0.016\%$ very nearly reach their equilibrium radius at 100% humidity (Alofs, 1978). From this equilibrium radius $r_{100}$, the value of $S_c$ can be determined using the following relation (Alofs, 1978):

$$S_c = 0.04/r_{100}, \quad (2)$$

where $S_c$ is in percent and $r_{100}$ is in micrometers.

One difficulty of the isothermal procedure concerns the question of how to calibrate the OPC for particles having the same index of refraction $m$, as does water ($m = 1.33$). Generally, OPC are calibrated using latex spheres with $m \approx 1.6$, but apparently no suitable means of generating a calibration aerosol with $m = 1.33$ has been developed. Theoretical calculations of OPC responses at various values of $m$ have been presented by Cooke and Kerker (1975). In the present investigation these calculations are used together with latex aerosol calibration data, in order to estimate the response of the OPC at $m = 1.33$.

Cooke and Kerker's calculations are performed for several commercial OPC, including the Royco 245 and Climet 201. Since the Royco 245 and the Royco 225 have identical optics, the two OPC used in the present investigation are included. Their calculations include $m = 1.33$ and 1.70. Unfortunately, $m = 1.60$, the index of refraction of latex, is not included. This complicates our task, and as a result three different calibration curves are eventually used, none of which is expected to be the correct curve for $m = 1.33$. However, it is expected that these curves taken together define the band of uncertainty due to index of refraction effects.

The manufacturers of the Royco and the Climet OPC each provide a calibration curve, obtained by calibration with latex aerosols. These two curves are each denoted curve A, and consist of a plot of response (plus voltage) on the ordinate and particle size on the abscissa. The pulse height analyzer (PHA) inside the Royco and the Climet OPC do not have a sufficient number of channels to conveniently use for the present application and therefore a Nuclear Data[7] Model 220 PHA was used instead. The effect of using a different PHA is to change the response gain of the OPC, which then slightly shifts the calibration curve up or down. However, the vertical scale on the plot is logarithmic and thus the shape of the curve does not change. Therefore to reestablish the calibration curve after switching PHA, it is only necessary to calibrate the OPC and the PHA for one size latex aerosol. In the present investigation, this was done using 2.02 $\mu$m diameter polyvinyltoluene latex spheres with $m = 1.5793$, obtained from Dow Chemical, Midland, Michigan. As a check, calibration

[7] Nuclear Data Inc., Golf and Meachan Roads, Schaumberg, IL 60162.

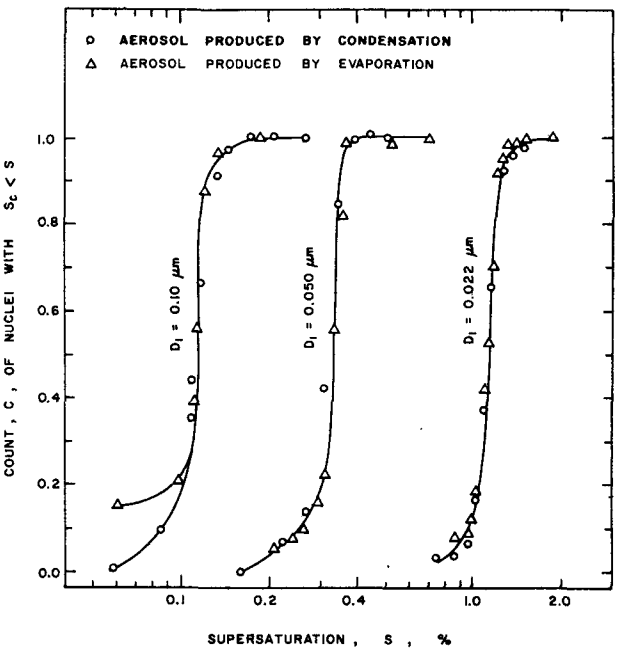


FIG. 8. Selected data from the temperature sweep experiments.

was also performed with 0.945 $\mu$m diameter polystyrene latex spheres with $m = 1.5905$, obtained from the same sources. For the Climet OPC, the two sizes of latex particles gave the same calibration curve. However, for the Royco OPC, the signal to noise ratio at 0.945 $\mu$m diameter was unacceptably low, and therefore the Royco OPC was useful for only larger sizes. It should be pointed out that the high noise in the Royco was due to dirt accumulated on the optics during hundreds of hours of use and is not an inherent deficiency of the instrument.

Calibration curves B and C are the Cooke and Kerker curves at $m = 1.33$ and $m = 1.70$, respectively. The two curves were simultaneously shifted up or down so that our calibrated response for 2.02 $\mu$m diameter latex agreed with the $m = 1.70$ curve.

To obtain values of $r_{100}$ from the isothermal procedure, NaCl aerosols of known dry size are passed through the isothermal CFD, and the most frequent pulse height from the OPC is determined with the PHA. This pulse height is converted into a value of water drop size, $r_{100}$, using the three calibration curves. Thus curve A corresponds to assuming that the water drops have the same index of refraction as do the latex particles ($m = 1.60$). Curve B corresponds to assuming that both the water drops and the latex calibration aerosol have $m = 1.70$. Curve C corresponds to assuming that the water drops have $m = 1.33$ and the latex particles have $m = 1.70$. As stated above, none of these sets of assumptions are correct, but the maximum deviation between the correct curve and any of the three curves is expected to be smaller than the deviation among the three curves.

## 8. Results of the temperature sweep procedure

Fig. 8 shows a plot of selected data from the temperature sweep procedure. The ordinate shows the count $C$ of nuclei with $S_c < S$, normalized with respect to the maximum count obtained ruring the temperature sweep. The abscissa shows the operating supersaturation $S$ of the CFD. Data is shown for aerosols with three different size settings of the classifier, *viz.*, $D_1 =$ 0.022, 0.05 and 0.10 $\mu$m. Data for aerosols produced by both generating techniques are shown and are distinguished.

The value of $S$ at $C=0.5$ is taken to be $S_c$. The values of $S$ at $C=0.8$ and $C=0.2$ are denoted $S_{0.8}$ and $S_{0.2}$, respectively. Let $\Delta S$ be defined by the equation

$$2(\Delta S) = S_{0.8} - S_{0.2}. \quad (3)$$

An electrostatic classifier and CFD having infinite resolution would give a step function in Fig. 8 for a, truly monodisperse aerosol. Bearing this in mind $\Delta S/S_c$ can be seen to be a measure of the combined resolution of the classifier and the CFD.

Table 1 shows all of the temperature sweep data for aerosols produced by condensation. The first column shows $D_1$, the size setting of the classifier. The second column shows $Q_3$, the filtered air flow rate in the classifier. The classifier aerosol flow rate, $Q_6$, was always 0.1 times $Q_3$. The third column shows the dew point of the air supply to the aerosol generator (Fig. 1). In cases where the dew point is below $-21$°C, the air supply was from the dry-air-supply system of the University of Missouri cloud simulation chamber facility. In these cases the dew point was measured with a Cambridge Systems[8] Model 992-Cl dew-point hygrometer. In cases where the dew point is higher, the air supply was room air, and on the basis of sporatic sling psychrometer measurements, the dew point was estimated to be 10°C±3°C. The fourth column in Table 1 shows which thermal diffusion chamber (CFD) was used. Recall that CFD #1 has a Royco OPC and CFD #2 has a Climet OPC. The fifth column shows $S_c$, and the last column shows $\Delta S/S_c$, with $\Delta S$ defined by Eq. (3).

TABLE 1. Data from nucleation experiments with aerosol from the condensation generator. See text for definition of terms.

| $D_1$ ($\mu$m) | $Q_3$ ($\ell$ min$^{-1}$) | Dew point (°C) | CFD (No.) | Date 1978 | $S_c$ (%) | $\Delta S/S_c$ |
|---|---|---|---|---|---|---|
| 0.022 | 20 | 10±3 | 2 | 08/31 | 1.09 | 0.031 |
| 0.022 | 20 | 10±3 | 2 | 09/28 | 1.10 | 0.068 |
| 0.022 | 20 | −21 | 2 | 11/15 | 1.10 | 0.036 |
| 0.022 | 6 | −38 | 2 | 12/15 | 1.05 | 0.046 |
| 0.022 | 6 | 10±3 | 2 | 12/15 | 1.05 | 0.046 |
| | | | | Average | 1.08 | 0.045 |
| 0.050 | 20 | 10±3 | 2 | 08/04 | 0.32 | 0.094 |
| 0.050 | 20 | 10±3 | 2 | 09/07 | 0.35 | 0.078 |
| 0.050 | 6 | 10±3 | 2 | 10/11 | 0.33 | 0.075 |
| 0.050 | 6 | 10±3 | 2 | 10/13 | 0.35 | 0.071 |
| 0.050 | 20 | 10±3 | 2 | 11/30 | 0.34 | 0.044 |
| 0.050 | 20 | −37 | 1 | 12/07 | 0.33 | 0.091 |
| 0.050 | 20 | 10±3 | 1 | 12/07 | 0.34 | 0.074 |
| | | | | Average | 0.337 | 0.075 |
| 0.10 | 6 | 10±3 | 1 | 10/20 | 0.110 | 0.146 |
| 0.10 | 6 | 10±3 | 2 | 11/29 | 0.135 | 0.066 |
| 0.10 | 6 | 10±3 | 2 | 11/29 | 0.125 | 0.120 |
| 0.10 | 20 | 10±3 | 2 | 11/29 | 0.130 | 0.096 |
| 0.10 | 6 | −35 | 2 | 12/08 | 0.125 | 0.080 |
| 0.10 | 6 | 10±3 | 2 | 12/08 | 0.135 | 0.140 |
| | | | | Average | 0.127 | 0.108 |

TABLE 2. As in Table 1 except from the evaporation generator.

| $D_1$ ($\mu$m) | $Q_3$ ($\ell$ min$^{-1}$) | CFD (No.) | Date 1978 | $S_c$ (%) | $\Delta S/S_c$ |
|---|---|---|---|---|---|
| 0.022 | 20 | 2 | 10/18 | 1.10 | 0.068 |
| 0.022 | 6 | 2 | 11/21 | 1.00 | 0.035 |
| 0.022 | 6 | 1 | 11/21 | 1.15 | 0.046 |
| 0.022 | 6 | 1 | 11/21 | 1.15 | 0.046 |
| 0.022 | 6 | 2 | 11/21 | 1.00 | 0.035 |
| | | | Average | 1.08 | 0.046 |
| 0.050 | 20 | 2 | 10/19 | 0.33 | 0.106 |
| 0.050 | 20 | 2 | 10/24 | 0.33 | 0.061 |
| 0.050 | 20 | 1 | 10/24 | 0.31 | 0.076 |
| 0.050 | 20 | 1 | 10/24 | 0.28 | 0.054 |
| 0.050 | 20 | 1 | 10/24 | 0.30 | 0.100 |
| 0.050 | 6 | 2 | 10/24 | 0.33 | 0.046 |
| 0.050 | 6 | 2 | 11/22 | 0.29 | 0.035 |
| 0.050 | 6 | 1 | 11/22 | 0.35 | 0.086 |
| | | | Average | 0.315 | 0.071 |
| 0.10 | 20 | 2 | 10/04 | 0.110 | 0.082 |
| 0.10 | 6 | 2 | 11/21 | 0.110 | 0.136 |
| 0.10 | 6 | 2 | 11/22 | 0.115 | 0.10 |
| 0.10 | 6 | 2 | 11/22 | 0.115 | 0.10 |
| | | | Average | 0.112 | 0.105 |

Table 2 is similar to Table 1 but is for aerosols from the evaporation generator. Comparing Tables 1 and 2, it can be seen that for $D_1 = 0.022$ $\mu$m, both aerosols give the same average value of $S_c$, *viz.*, $S_c = 1.08\%$. For $D_1 = 0.050$ $\mu$m, the condensation aerosol shows $S_c = 0.337\%$, and the evaporation aerosol shows $S_c = 0.315\%$. This difference is in the direction which would indicate an energy barrier for dry NaCl in accord with the hypothesis of Section 1. However, in view of the fact that the difference is less than the scatter in $S_c$ shown by each aerosol, we interpret the difference to be statistically insignificant. At $D_1 = 0.10$ $\mu$m, the condensation aerosol shows $S_c = 0.127\%$, and the evaporation aerosol shows $S_c = 0.112\%$, which again is a difference in such a direction as to indicate an energy barrier. However, the difference is again judged to be so small as to be statistically insignificant.

Now focusing attention on the average values of $\Delta S/S_c$, it can be seen from Tables 1 and 2 that $\Delta S/S_c$ increases as $D_1$ increases. Qualitatively, this is to be expected because the resolution of both the classifier and the CFD is best for the small particles. For the

[8] Cambridge Systems, Inc., 50 Hung Street, Newton, MA 02158.

classifier, this is because as $D_1$ increases, $R$ decreases (Fig. 4). For the CFD, this is because for larger $D_1$, there is increased difficulty in distinguishing the haze nuclei from the active nuclei (Alofs, 1978).

The overall average of $\Delta S/S_c$ is 0.075 for the data of Tables 1 and 2. It is interesting to consider how much of $\Delta S/S_c$ is due to the classifier versus that which is due to the CFD. Assuming the classifier is behaving ideally, it would have a triangular transfer function $\Omega$ such that $\Delta Z/Z_p=0.1$ (Section 4). Integrating $\Omega$ with respect to $Z$, one obtains a cumulative transfer function $\beta$. The value of $\beta$ is zero for $Z<Z_p-\Delta Z$, rises nonlinearly with $Z$ in the range from $Z_p-\Delta Z$ to $Z_p+\Delta Z$ and is unity for $Z>Z_p+\Delta Z$. The value of $Z$ at $\beta=0.2$ is denoted $Z_{0.2}$ and at $\beta=0.8$ is $Z_{0.8}$. Then it can be shown that $Z_{0.8}-Z_{0.2}=0.74\Delta Z=0.074Z_p$. In analogy to Eq. (3), let $\Delta Z_c$ be defined by:

$$2(\Delta Z_c)=Z_{0.8}-Z_{0.2}. \tag{4}$$

Thus $\Delta Z_c=0.037Z_p$. By consulting a mobility table for singly charged particles, it can be determined that a 3.7% change in mobility corresponds to about a 2.0% change in particle diameter in the size range 0.01–0.10 $\mu$m. Now consulting the Köhler equations, it can be determined that a 2% change in particle size corresponds to a 3.5% change in $S_c$. Thus the value of $\Delta S/S_c$ attributable to an ideal classifier is $\Delta S/S_c=0.035$. This then shows that about half of the average experimental value of $\Delta S/S_c$ is due to other considerations, either non-ideal behavior of the classifier, or the resolution of the CFD. Incidentally, it should be pointed out that the scatter in the value of $\Delta S/S_c$ is very large, and the reason for this scatter is unknown. It would not seem to be due to wandering of the aerosol stream in the CFD from the midplane, as this would cause both $\Delta S/S_c$ and $S_c$ to go up, whereas the data shows no such correlation.

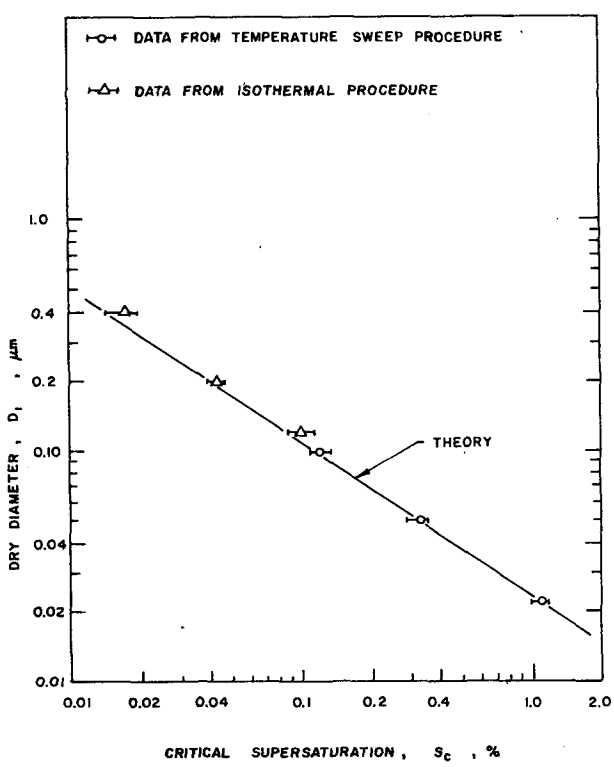


FIG. 9. Average values of $S_c$ measured in the nucleation experiments, versus dry size of the monodisperse NaCl aerosols.

TABLE 3. Data from the isothermal procedure.

| | | | |
|---|---|---|---|
| $D_1$ ($\mu$m) | 0.13 | 0.20 | 0.40 |
| $S_c$ (% Köhler) | 0.0753 | 0.0395 | 0.0140 |
| $r_{100}$ ($\mu$m, Köhler) | 0.531 | 1.01 | 2.865 |
| $S_c$ (%, Royco) | | | |
| Curve A | — | 0.046 | 0.014 |
| Curve B | — | 0.044 | 0.014 |
| Curve C | — | 0.047 | 0.019 |
| $S_c$ (%, Climet) | | | |
| Curve A | 0.100 | 0.043 | 0.018 |
| Curve B | 0.078 | 0.042 | 0.019 |
| Curve C | 0.082 | 0.040 | 0.016 |

Before leaving Tables 1 and 2, it is noted that $Q_3$, the classifier filtered air flow rate, did not noticeably influence $S_c$. This gives some confidence in the classifier flowmeters, voltmeters, and aerodynamic flow. It is also noted that $S_c$ did not depend on which of the two CFD was used. From Table 1, it can be seen that the dew point of the air supply for the condensation generator did not influence $S_c$.

The circles in Fig. 9 show the average value of $S_c$ from Table 1 and Table 2, plotted as a function of $D_1$. The error bars denote the maximum scatter in $S_c$ from these tables. The straight line in Fig. 9 is the theoretical result given by Köhler equations. This line has the equation

$$D_1=0.0232S_c^{-\frac{3}{2}}. \tag{5}$$

Eq. (5) was not obtained directly from the Köhler equations, because a full description of how these equations were solved would require a separate paper. Therefore, Eq. (5) was obtained by carefully measuring the coordinates of the Köhler theory line in Fig. 8 of the paper by Gerber *et al.* (1977). Moreover, Eq. (5) agrees very well with Table X in the article by Hänel (1976). It can be seen from Fig. 9 that the temperature sweep data is in good agreement with the Köhler theory.

## 9. Results of the isothermal procedure

Table 3 shows the results of the isothermal procedure experiments. The first line shows the dry size of the NaCl aerosols tested. In each case the evaporation aerosol generator was used. The second line shows the values of $S_c$, obtained from the Köhler theory [Eq. (5)]. The third line shows $r_{100}$, the equilibrium radius at 100% humidity, obtained from Eq. (2) and the values of $S_c$ on line 2. The remaining lines show the values of $S_c$ obtained from the measurements of $r_{100}$ with the

Royco and Climet OPC, and using Eq. (2) to convert into values of $S_c$. Curves A, B and C denote the different response curves used, corresponding to various assumed values of index of refraction, as described in Section 7.

The maximum deviation between the experimental values of $S_c$ in Table 3 is 36%. By coincidence, the maximum deviation between the experimental and Köhler values is also 36%. The first deviation represents the uncertainty in the experiment due to index of refraction effects. The second deviation indicates the accuracy to which the Köhler theory has been experimentally verified. Although a 36% uncertainty is large, it should be remembered that the data covers almost a decade range in $S_c$ values. Fig. 9 shows a plot of the values of $S_c$ from Table 3. The triangles show the average $S_c$ and the bars denote the lower and upper limits from Table 3. In the context of Fig. 9, the 36% uncertainty is not so large as to render the procedure useless.

## 10. Conclusions

The nucleation experiments with monodisperse NaCl aerosols showed good agreement with the Köhler theory relating the critical supersaturation $S_c$ to dry size. Aerosols produced by condensing NaCl showed nearly the same $S_c$ as those produced by evaporating aqueous NaCl solution droplets. This indicates that if there is an energy barrier in going from a dry NaCl particle to a solution droplet, this energy barrier is small; small in the sense that the $S$ to overcome this barrier is smaller than the $S_c$ given by the Köhler theory. These results also indicate that there is no significant contamination of the evaporated aerosol by surface active materials during the course of our experiments. The fact that the evaporation aerosol particles are cubical crystals and the condensation aerosols are amorphous spheres is shown to make little or no difference in the nucleation threshold.

The investigation also gives insights into the performance of the equipment used. The commercial electrostatic classifier gave internally consistent results when the flow rates were varied. The pattern of salt deposits observed when cleaning the classifier showed angular non-uniformity, indicating that the aerodynamics of the inlet system could be improved. As to the resolution of the classifier, the ideal value for the quantity $\Delta S/S_c$ is 0.035. The average value of $\Delta S/S_c$ measured with the continuous flow thermal diffusion chamber (CFD) was 0.075, but it is not known how much of this $\Delta S/S_c$ is due to the resolution of the classifier versus how much is due to the TDC.

The CFD was operated in the isothermal mode for monodisperse NaCl aerosol of 0.13, 0.2 and 0.4 $\mu$m diameter. The uncertainty in $S_c$ due to index of refraction sensitivity in the OPC was found to be 36%. Within this range of uncertainty, the data from the isothermal mode agreed with Köhler theory.

*Acknowledgments.* The major encouragement for developing the aerosol generation facility was provided by J. L. Kassner, Jr. The condensation aerosol generator has been under development for some five years at this laboratory. The first work on it was done by S. Shahriari, with successive contributions by J. Podzimek and J. F. Stampfer.

The recent financial support for this work has been from Grant NSF-ATM75-21421 from the Atmospheric Sciences Section, National Science Foundation and Grant ONR-N00014-75-C-0182 from the Office of Naval Research.

## REFERENCES

Alofs, D. J., 1978: Performance of a dual range cloud nucleus counter. *J. Appl. Meteor.*, **17**, 1286–1297.

Cooke, D. D., and M. Kerker, 1975: Response calculations for light-scattering aerosol particle counters. *Appl. Opt.*, **14**, 734–739.

Derjaguin, B. V., I. S. Kurghin, L. A. Rosenzweig and V. A. Fedoseyev, 1971: Study of passivation of condensation growth of water and salt solutions. *Aerosol Sci.*, **2**, 261–274.

Espenscheid, W. F., E. Matijević and M. Kerker, 1964: Aerosol studies by light scattering. III Preparation and particle size analysis of sodium chloride aerosols of narrow size distribution. *J. Phys. Chem.*, **68**, 2831–2842.

Fleagle, R. G., and J. A. Businger, 1963: *An Introduction to Atmospheric Physics*. Academic Press, 346 pp.

Fuchs, N. A., 1964: *The Mechanics of Aerosols*. Pergamon Press, 408 pp.

——, and A. G. Sutugin, 1966: Generation and use of monodisperse aerosols. *Aerosol Science*, C. N. Davies, Ed., Academic Press, 468 pp.

Gerber, H. E., W. A. Hoppel and T. A. Wojciechowski, 1977: Experimental Verification of the theoretical relationship between size and critical supersaturation of salt nuclei. *J. Atmos. Sci.*, **34**, 1836–1841.

Hänel, G., 1976: The properties of atmospheric aerosol particles as functions of the relative humidity at thermodynamic equilibrium with the surrounding moist air. *Advances in Geophysics*, Vol. 19, H. E. Landsberg and J. Van Mieghem, Eds., Academic Press, 312 pp.

Hoppel, W. A., 1978: Determination of the aerosol size distribution from the mobility distribution of the charged fraction of aerosols. *J. Aerosol. Sci.*, **9**, 41–54.

Kerker, M., 1975: Laboratory generation of aerosols. *Advances in Colloid Interface Science*, Vol. 5, Academic Press, 105–172.

Kitani, S., and S. Ouchi, 1967: Preparation of monodisperse aerosols of sodium chloride. *J. Colloid Interface Sci.*, **23**, 200–202.

Knight, C. A., 1971: A note on the action of hygroscopic cloud nuclei. *J. Atmos. Sci.*, **28**, 1296–1297.

Knutson, E. O., and K. T. Whitby, 1975: Aerosol classification by electric mobility: apparatus, theory, and applications. *J. Aerosol Sci.*, **6**, 443–451.

Liu, B. Y. H., and D. Y. H. Pui, 1974a: A submicron aerosol standard and the primary, absolute calibration of the condensation nuclei counter. *J. Colloid Interface Sci.*, **47**, 155–171.

——, and ——, 1974b: Equilibrium bipolar charge distribution of aerosols. *J. Colloid Interface Sci.*, **49**, 305–312.

——, ——, A. W. Hogan and T. A. Rich, 1975: Calibration of the Pollak Counter with monodisperse aerosols. *J. Appl. Meteor.*, **14**, 46–51.

Matijević, E., K. F. Schultz and M. Kerker, 1962: Light scattering of coated aerosols. II. Scattering by linolenic acid aerosols. *J. Colloid Sci.*, **17**, 26–38.

——, W. F. Espenscheid and M. Kerker, 1963: Aerosols consisting of spherical particles of sodium chloride. *J. Colloid Sci.*, **18**, 91–94.

May, K. R., 1973: The collision nebulizer: Description, performance and application. *J. Aerosol Sci.*, **4**, 235–243.

Podzimek, J., and A. N. Saad, 1975: Retardation of condensation nuclei growth by surfactant. *J. Geophys. Res.*, **80**, 3386–3392.

Pruppacher, H. R., and J. D. Klett, 1978: *Microphysics of Clouds and Precipitation*. D. Reidel, 714 pp.

Winkler, P., and C. Junge, 1972: The growth of atmospheric aerosol particles as a function of humidity. *J. Rech. Atmos.*, **6**, 617–638.